Flood Impacts on Net Ecosystem Exchange in the Midwestern and Southern United States in 2019

Nikolay Balashov[1], Lesley E Ott[1], Brad Weir[1], Sourish Basu[1], Kenneth J Davis[2], Natasha L Miles[2], Anne M Thompson[3], and Ryan M Stauffer[3]

[1]Goddard Space Flight Center
[2]The Pennsylvania State University
[3]NASA Goddard Space Flight Center

November 24, 2022

Abstract

Climate extremes such as droughts, floods, heatwaves, frosts, and windstorms add considerable variability to the global year-to-year increase in atmospheric CO2 through their influence on terrestrial ecosystems. While the impact of droughts on terrestrial ecosystems has received considerable attention, the response to flooding events of varying intensity is poorly understood. To improve upon such understanding, the impact of the 2019 US flooding on regional CO2 vegetation fluxes is examined in the context of 2017-2018 years when such precipitation anomalies are not observed. CO2 is simulated with NASA's Global Earth Observing System (GEOS) combined with the Low-order Flux Inversion (LoFI), where fluxes of CO2 are estimated using a suite of remote sensing measurements including greenness, night lights, and fire radiative power and bias corrected based on in situ observations. Net ecosystem exchange CO2 tracer is separated into the three regions covering the Midwest, South, and Eastern Texas and adjusted to match CO2 observations from towers located in Iowa, Mississippi, and Texas. Results indicate that for the Midwestern region consisting primarily of corn and soybeans crops, flooding contributes to a 15-25% reduction of net carbon uptake in May-September of 2019 in comparison to 2017 and 2018. These results are supported by independent reports of changes in agricultural activity. For the Southern region, comprised mainly of non-crop vegetation, net carbon uptake is enhanced in May-September of 2019 by about 10-20% in comparison to 2017 and 2018. These outcomes show the heterogeneity in effects that excess wetness can bring to diverse ecosystems.

Flood Impacts on Net Ecosystem Exchange in the Midwestern and Southern United States in 2019

Nikolay V. Balashov[1,2], Lesley E. Ott[1], Brad Weir[1,3], Sourish Basu[1,2], Kenneth J. Davis[4,5], Natasha L. Miles[4], Anne M. Thompson[6,7], Ryan M. Stauffer[6]

[1]NASA Global Modeling and Assimilation Office (GMAO), Goddard Space Flight Center, Greenbelt, MD, 20771, USA
[2]Earth System Science Interdisciplinary Center, University of Maryland, College Park, MD, USA
[3]Goddard Earth Sciences Technology and Research, Universities Space Research Association, 7178 Columbia Gateway Drive, Columbia, MD, 21046, USA
[4]Department of Meteorology and Atmospheric Science, The Pennsylvania State University, University Park, PA 16802, USA
[5]Earth and Environmental Systems Institute, The Pennsylvania State University, University Park, PA 16802, USA
[6]Earth Sciences Division, NASA Goddard Space Flight Center, Greenbelt, MD, 20771, USA
[7]University of Maryland-Baltimore County, JCET, Baltimore, MD 21228

Key Points:

- A devastating flood occurred in 2019 over the Midwestern and Southern regions of the US significantly affecting ecosystem carbon cycling
- Net ecosystem exchange is examined in the flood-effected areas with NASA's GEOS modeling system from 2017 through 2019
- The 2019 floods caused a net reduction in Midwestern crop carbon uptake and smaller net increase in non-crop uptake in Southern states

Corresponding author: Nikolay V. Balashov, `nikolay.v.balashov@nasa.gov`

Abstract

Climate extremes such as droughts, floods, heatwaves, frosts, and windstorms add considerable variability to the global year-to-year increase in atmospheric CO_2 through their influence on terrestrial ecosystems. While the impact of droughts on terrestrial ecosystems has received considerable attention, the response to flooding events of varying intensity is poorly understood. To improve upon such understanding, the impact of the 2019 US flooding on regional CO_2 vegetation fluxes is examined in the context of 2017-2018 years when such precipitation anomalies are not observed. CO_2 is simulated with NASA's Global Earth Observing System (GEOS) combined with the Low-order Flux Inversion (LoFI), where fluxes of CO_2 are estimated using a suite of remote sensing measurements including greenness, night lights, and fire radiative power and bias corrected based on in situ observations. Net ecosystem exchange CO_2 tracer is separated into the three regions covering the Midwest, South, and Eastern Texas and adjusted to match CO_2 observations from towers located in Iowa, Mississippi, and Texas. Results indicate that for the Midwestern region consisting primarily of corn and soybeans crops, flooding contributes to a 15-25% reduction of net carbon uptake in May-September of 2019 in comparison to 2017 and 2018. These results are supported by independent reports of changes in agricultural activity. For the Southern region, comprised mainly of non-crop vegetation, net carbon uptake is enhanced in May-September of 2019 by about 10-20% in comparison to 2017 and 2018. These outcomes show the heterogeneity in effects that excess wetness can bring to diverse ecosystems.

Plain Language Summary

The primary driver of the climate change is the fossil fuel emissions of carbon dioxide (CO_2). However, only a fraction of emitted CO_2 stays in the atmosphere as the rest is absorbed by the global ecosystem, which includes land and ocean. Recently, due to the growing concentration of CO_2 in the atmosphere and the change in climate the land component of the ecosystem has been experiencing an increased variability in its ability to uptake CO_2. This variability is partially controlled by the extreme weather events such as droughts and floods. In this work a devastating flood of 2019 in the Midwestern and Southern US is examined with respect to its effects on the land ecosystem and its ability to absorb CO_2. The analysis is performed with a model that simulates CO_2 concentrations, which are improved using the CO_2 observations from towers. The simulation allows to compare absorbed CO_2 over the years of 2017-2019 and the results indicate that at the affected region 2019 absorbed less CO_2 than years 2017 and 2018. As humans are hurriedly developing strategies to sequester carbon from the atmosphere, effects of floods on the carbon cycle at land ecosystems must be taken into the consideration.

1 Introduction

Understanding the future evolution of the carbon cycle is crucial to improve climate change predictions (Frank et al., 2015). Studies show that climate extremes (i.e., extreme weather events) have a noticeable effect on terrestrial ecosystems influencing the cycling of carbon and thereby affecting global atmospheric CO_2 concentrations (Reichstein et al., 2013; Frank et al., 2015). These extremes are characterized by meteorological phenomena such as droughts, floods, heat waves, frosts, and windstorms (Reichstein et al., 2013). While general understanding regarding how these extremes affect the global carbon cycle exists, each case presents a unique challenge that may deviate from expected behavior. To better understand the effects of climate extremes on carbon exchange between terrestrial ecosystem and atmosphere, detailed analysis of relevant case studies is required.

Droughts are common extreme weather events that impact terrestrial ecosystem carbon processes and are relatively well studied (van der Molen et al., 2011). In the time of drought, the ability of an ecosystem to consume CO_2 decreases (Frank et al., 2015; Schwalm et al., 2012). While the impact of droughts on terrestrial ecosystem has received considerable attention over the recent years, the response of an ecosystem to flooding events is intricate and ambiguous (Zaerr, 1983; Miyata et al., 2000; Knapp et al., 2008; Dušek et al., 2009; Zona et al., 2012; Dalmagro et al., 2019). As the climate changes, climate models predict an increase in precipitation for midlatitude regions, thereby increasing the likelihood of flooding events affecting these ecosystems (Knapp et al., 2008; Zhang & Villarini, 2021). Therefore, it is imperative to better understand how the potential increase in flooding events may affect future carbon budget.

The effects of flooding on carbon exchange in the terrestrial ecosystem depends on the type of vegetation affected. Wetlands tend toward storing less atmospheric carbon during flooding as photosynthesis weakens; however, annual Net Ecosystem Exchange (NEE) may not change much as ecosystem respiration (RE) also decreases (Han et al., 2015). Typically, during a growing season trees, shrubs, and grasses support a net uptake of atmospheric CO_2 and continue to do so even during some flooding, but it is not exactly clear how an increase in the magnitude of that flooding may alter this process (Kramer et al., 2008; Bourtsoukidis et al., 2014; Detmers et al., 2015). Croplands, however, are easily susceptible to waterlogging and tend to be a net source of atmospheric carbon when flooding occurs (Rosenzweig et al., 2002; Ahmed et al., 2013; Yin et al., 2020; Yildirim & Demir, 2022). Although the majority of CO_2 that is initially absorbed by croplands is eventually released back into the atmosphere, the cropland soils have the capacity to sequester atmospheric CO_2 and their ability to hold carbon is critically important for reducing global atmospheric CO_2 levels (Paustian et al., 2000; Follett, 2001; Zomer et al., 2017). Also, extreme precipitation events may cause topsoil erosion leading to additional carbon emissions into the atmosphere (Hilton et al., 2008; Dinsmore et al., 2013; Lal, 2019). To further the knowledge of the effects of flooding on ecosystem carbon fluxes, the spring/early summer Midwestern and central Southern US flooding events of 2019 are investigated.

Heavy precipitation in the spring/early summer of 2019 resulted in widespread flooding of the Upper Mississippi River Basin and the surrounding regions causing damages in the range of 2-3 billion US dollars (Neri et al., 2020; Reed et al., 2020). The focus of this study is on the Midwest (M) and South (S and T, Figure 1), where the flood affected areas with different types of vegetation. In the Midwest vegetation primarily consists of croplands such as maize (corn) and soybeans, while in the South there are mainly forests transitioning to prairies in Eastern Texas (Figure 1). The main objective of this work is to examine the effects of the 2019 flood on the NEE of ecosystems in these regions in comparison to years with no anomalous precipitation (2017 and 2018).

Previously, Yin et al. (2020) showed the ability to quantify Midwest atmospheric CO_2 and Midwest croplands gross primary production (GPP) anomalies during the abovementioned 2019 flood using XCO_2 measurements from the Orbiting Carbon Observatory 2 (OCO-2) and solar-induced chlorophyll fluorescence (SIF) derived from the TROPOspheric Monitoring Instrument (TROPOMI). Comparing 2019 to 2018, their results indicated reduction in the Midwest cropland GPP of -0.21 PgC in June and July and partial recovery of 0.14 PgC in August and September. They also noted a flood-forced 3-week delay in the planting date of crops across much of the area. The present study builds upon Yin et al. (2020) by analyzing the NEE of the flood-affected region in 2019, expanding to different vegetation types, and extending the comparison by including the additional year of 2017. The focus is on better understanding of the 2019 flooding event and its impact on agricultural ecosystems. Also, the performance of near real time carbon modeling tools is assessed and implications for carbon monitoring are discussed.

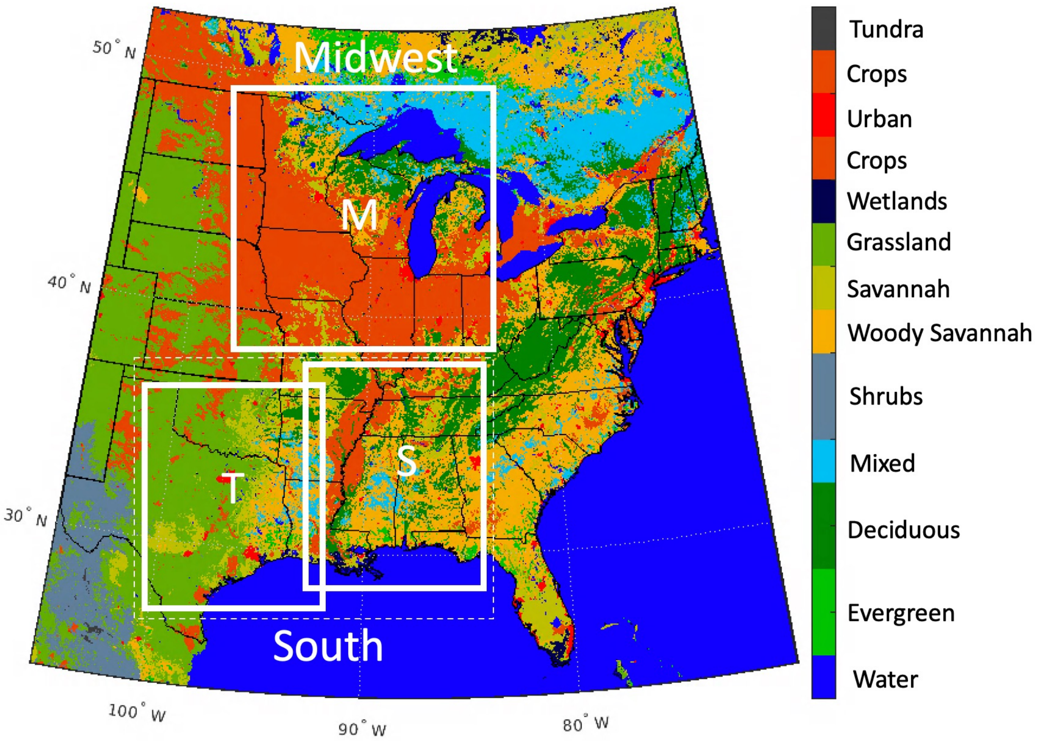

Figure 1. Land cover map of the Eastern Conterminous United States (CONUS) derived from Moderate Resolution Imaging Spectroradiometer (MODIS). White squares indicate regions affected by the anomalous precipitation and are the focus of this study. Capital letter M indicates the Midwest region, while capital letters S (South) and T (Texas) represent regions of the South (for more details see Data and Methods section).

2 Data and Methods

2.1 MERRA-2 and Evidence of Flooding

To map out regions of the flooding in 2019, soil moisture and precipitation data from the Modern-Era Retrospective analysis for Research and Applications, Version 2 (MERRA-2) are used (Gelaro et al., 2017). Soil moisture is described by the ground wetness variable for the 0-5 cm layer of soil. The variable is dimensionless in units of relative saturation ranging from 0 to 1, where value of 1 indicates completely saturated soil. Bias corrected MERRA-2 precipitation (mm) comprised of background data products [such as Goddard Earth Observing System Model, version 5 (GEOS-5) or Forward Processing system for Instrument Teams (FP-IT)] and observations [i.e., Global Precipitation Climatology Project (GPCP)] is utilized (Reichle, Draper, et al., 2017; Reichle, Liu, et al., 2017). For both soil moisture and precipitation 2017-2019 anomalies with respect to 1981-2010 climatology are calculated over the region of interest.

2.2 Crop Data

Since croplands contribute significantly to the carbon cycle of the M region, 2017-2019 United States Department of Agriculture (USDA) crop planting data are analyzed for corn (maize) and soybeans - the two most common crops in the US Midwest. In this study, three attributes, which are crop planting progress, acres planted, and grain yield, of corn and soybeans from years 2017-2019 are compared. The following states are analyzed here: Illinois, Indiana, Iowa, Kansas, Michigan, Minnesota, Missouri, Nebraska, Ohio, South Dakota, and Wisconsin. The data is taken from National Agriculture Statistics Service provided by USDA (`https://quickstats.nass.usda.gov/`).

2.3 CO_2 Data

2.3.1 Optimization Data

The optimization of the GEOS model (described later in section 2.6) takes place in two different areas, the Midwest (M) and the South (broken down into two regions: S and T, Figure 1). The process of optimization consists of adjusting GEOS NEE CO_2 tracers from the 3 regions (M, S, and T) over the 3 years (2017-2019) in an attempt to match 5-day running mean of daily observations [averaged over the afternoon hours of 1500-1700 local standard time (LST)] from four in situ CO_2 towers located in each region of interest: West Branch, Iowa (WBI) in M, Magee, Mississippi (MS-01) in S, Grenada, Mississippi (MS-02) in S, and Moody, Texas (WKT) in T (see Figure 2).

The WBI tower is in the agricultural ecosystem (corn belt) of eastern Iowa and is part of the National Oceanic and Atmospheric Administration (NOAA) Earth System Research Laboratories/Global Monitoring Laboratory (ESRL/GML) tall tower network that is tasked with the goal of long-term carbon-cycle gas monitoring in the atmospheric boundary layer (ABL) of continental areas (Andrews et al., 2014; Schuldt et al., 2021). The location of the tower is ideal for CO_2 monitoring pertinent to the Midwestern croplands and hence is used here to analyze the effects of the 2019 flooding.

MS-01 and MS-02 towers are in Mississippi and were instrumented initially for the Gulf Coast Intensive, designed to characterize CO_2 in the southeastern region of the US and maintained through 2019 as part of the ACT-America project (Miles et al., 2018). The MS towers did not measure CO_2 simultaneously, so to represent the CO_2 of the region S, MS-01 is used for 2017 and MS-02 is used for 2018-2019. These towers are well suited for this study as the state of Mississippi was noticeably affected by the 2019 precipitation anomalies and consequential Mississippi river flooding (Price & Berkowitz, 2020).

Finally, WKT represents the T region of the South. Like WBI, the tower is part of the NOAA ESRL/GML tall tower network (Andrews et al., 2014). The location of the tower is optimal for capturing CO_2 variability in eastern Texas and western Louisiana, where the flooding of 2019 was also present.

2.3.2 Validation Data

Validation process with tower-based, airborne, and shipboard measurements is aimed at determining how well the towers used for the optimization act as a proxy for the regions of interest. The M region is validated with the Indianapolis Flux Experiment (INFLUX) background tower 1 that is located on the southwestern part of Indianapolis, the direction least influenced by the CO_2 emissions from the city (Davis et al., 2017). As in Iowa (where WBI is located), vegetation in Indiana mainly consists of crops, making it a good choice for the validation of the model optimizations at WBI. However, INFLUX tower 1 is immediately surrounded by forests, in contrast to WBI. The S and T regions are validated using towers in Millerville, Alabam (AL-01) and Monroe, Louisiana (LA-01). To be consistent with the optimization, 5-day running mean of daily observations (averaged over the afternoon hours of 1500-1700 LST) is utilized.

The airborne Atmospheric Carbon and Transport - America (ACT-America) and the shipboard Satellite Coastal and Oceanic Atmospheric Pollution Experiment (SCOAPE) campaigns in 2019 are also used for validation. ACT-America is an airborne NASA Earth Venture mission dedicated to improving the accuracy, precision, and resolution of atmospheric inverse estimates of CO_2 and CH_4 sources and sinks on a regional scale (Davis et al., 2021). The mission conducted 5 seasonal campaigns (including 2 summer campaigns) over the 2016-2019 period. For each campaign two aircraft (C-130 and B-200) were used to survey three different regions in the United States: The South, the Midwest, and the Mid-Atlantic. Data from the 2019 campaign covering the South and the Midwest is used, which occurred in June and July of 2019. Most of the flights took place in the period of 1100-1700 LST. For validation purposes the boundary layer [$\sim$330 m above ground level (AGL)] CO_2 was averaged for each of the selected flight days.

SCOAPE was a brief shipboard campaign investigating nitrogen dioxide (NO_2) emissions from oil and natural gas platforms in the Gulf from May 10-18 of 2019 (Thompson, 2020). Auspiciously there was a CO_2 instrument on board and the campaign was conducted at the same time as the flood of 2019. SCOAPE serves as a validation for the South region, specifically for the states of Louisiana, Mississippi, and Alabama. Averaged afternoon (1500-1700 LST) CO_2 measurements are used.

2.4 GEOS Model Configuration Including LoFI Flux Package

NASA GEOS general circulation model, constrained by MERRA-2 meteorology fields, with resolution of 0.5 by 0.625 degrees and 72 vertical layers (Molod et al., 2015) is utilized to simulate CO_2 over the region of interest (Weir et al., 2021). It includes the Low-order Flux Inversion (LoFI) package, which contains a compilation of carbon fluxes driven by remote-sensing land surface data (Ott et al., 2015; Weir et al., 2021) and a bias correction process designed to reproduce CO_2 mole fractions observed at NOAA's in situ network. There are five components to the mentioned LoFI flux package: NEE, biomass burning, fossil fuel combustion, ocean exchange, and an empirical land sink (bias correction of the fluxes).

NEE is computed using the Carnegie-Ames-Stanford Approach – Global Fire Emissions Dataset version 3 (CASA-GFED 3; Randerson et al., 1996; van der Werf et al., 2010) that estimates carbon fluxes using satellite-derived vegetation products and MERRA-2 meteorology. Biomass burning CO_2 emissions are derived with the Quick Fire Emissions Dataset (QFED; Koster et al., 2015), which is constructed using MODIS fire ra-

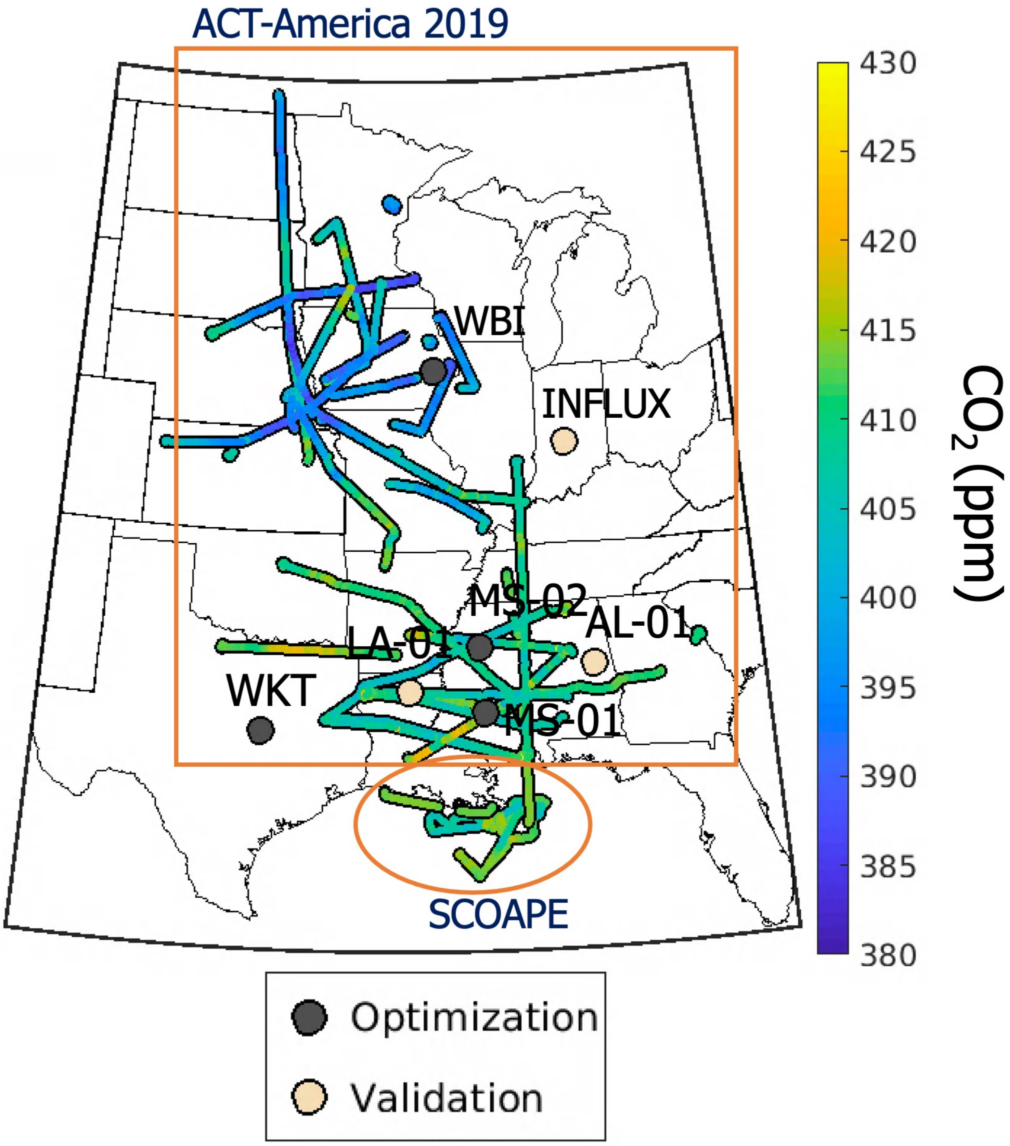

Figure 2. Observations that are used for the GEOS model optimization and validation. Aircraft transect and ship track mole fractions are shown inside the ABL and are used for validation. Towers are labeled by circles.

diative power (FRP) estimates in near real-time. Fossil fuel combustion is provided by the Open-source Data Inventory for Anthropogenic CO_2 (ODIAC; Oda & Maksyutov, 2015; Oda et al., 2018) that is based on disaggregated country-level fossil fuel CO_2 emission inventories using a global power plant database and satellite observations of nighttime lights. Ocean exchange of CO_2 is estimated using the differences between the partial pressure of CO_2 in seawater ($pCO^{sw}{}_2$) derived from the Takahasi et al. (2009) climatology and the partial pressure in the atmosphere ($pCO^{atm}{}_2$) taken from the NOAA marine boundary layer (MBL) reference (Masarie & Tans, 1995; Dlugokencky & Tans, 2016). An empirical land sink is applied as a bias correction to the collection of fluxes to constrain the modeled atmospheric CO_2 growth with the observed growth rates derived from the NOAA MBL reference (Weir et al., 2021).

2.5 Definition of Tagged Tracer Regions

Before the optimization an area that influences towers is designated using NOAA's Hybrid Single-Particle Lagrangian Integrated Trajectory (HYSPLIT) model backward trajectories (Stein et al., 2015). The trajectories are released backwards for every 6 hours for May through September of 2019 at the three optimization towers WBI, MS-02 (it is assumed MS-02 is representative of MS-01), and WKT from the level of the corresponding sensor (121-379 m AGL) using the North American Regional Reanalysis (NARR) meteorology. The approximate area influencing each tower combined with the MODIS Land Cover Climate Modeling Grid Product (MCD12C1) allow for the generation of CO_2 mole fraction tracer masks applied to tag regional NEE within GEOS that can be then used in the optimization (Figure 3). MCD12C1 is the reprojection of the tiled MODIS Land Cover Type Product (MCD12Q1) with the sub-pixel proportions of each land cover class in each 0.05° pixel and the aggregated quality assessment information from the International Geosphere-Biosphere Programme (IGBP) scheme (Sulla-Menashe & Friedl, 2018). MCD12C1 is regridded to the resolution of the LoFI of 0.5° by 0.625° to generate the appropriate masks of vegetation areas of interest while removing any urban and coastal environments.

2.6 Optimization Approach

To quantify the effects of 2019 flooding on regional vegetation, NEE is compared to the years 2017 and 2018. Though NEE is available from the LoFI flux package, it is possible that these fluxes are inaccurate because of the use of a highly simplified diagnostic vegetation model. To provide a better estimate, the NEE component of the LoFI collection, representative of the vegetation fluxes of a given area, is adjusted to minimize the model-observation CO_2 mole fraction difference. The optimization is independently performed for the three different regions of M, S, and T (Figure 3), where each region is characterized by its individual NEE CO_2 tracer based on the selected in situ towers.

The observed CO_2 mole fraction can be expressed in the following way:

$$CO2_{obs} = CO2_{model} + \Delta CO2, \tag{1}$$

where $CO2_{model}$ represents CO_2 from GEOS and $\Delta CO2$ is the mole fraction of CO_2 that needs to be added to the modeled mole fraction to arrive at the observed value. The $CO2_{model}$ term can be expanded as

$$CO2_{obs} = CO2_{ini} + CO2_{ocn} + CO2_{FF} + CO2_{fire} + CO2_{NEE}, \tag{2}$$

where $CO2_{ini}$ is an initial condition that consists of all the accumulated CO_2 at a particular model grid cell in the model prior to a May 1st of a given year (either 2017, 2018,

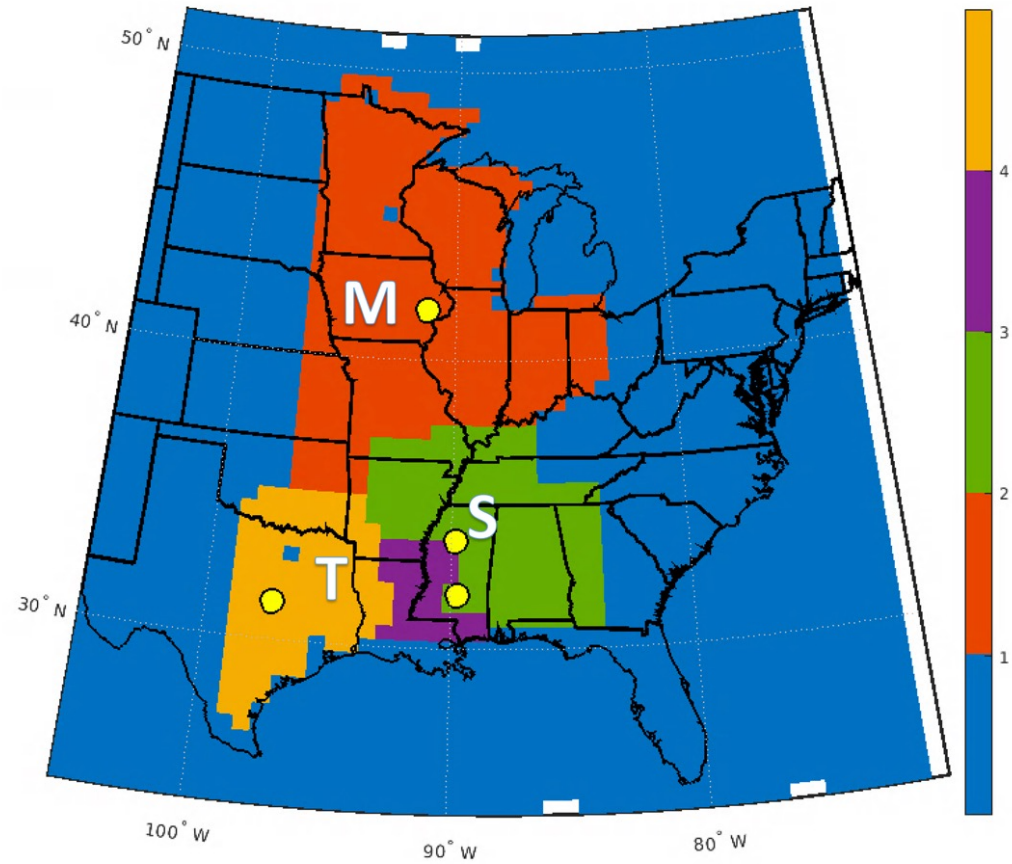

Figure 3. Masks for the optimization based on the backward HYSPLIT trajectories, where the blue region 0 shows areas not included as model CO_2 NEE tracers (the rest of the globe NEE), red region 1 influences WBI tower in Iowa and is labeled as M NEE CO_2 tracer, the green region 2 influences MS-01 and MS-02 towers in Mississippi and is labeled as S NEE CO_2 tracer, the purple region 3 influences both MS and WKT towers (part of both S and T NEE CO_2 tracers), and finally the yellow region 4 influences WKT tower in Texas and is labeled as T NEE CO_2 tracer. Yellow circles indicate towers used for optimization.

or 2019) and the rest of the right-hand terms are additions from ocean (OCN), fossil fuels (FF), fire, and NEE. In the current work it is hypothesized that NEE term is the most uncertain and that the $\Delta CO2$ term in equation (1) is mainly driven by the $CO2_{NEE}$ term. Therefore, it is the only term adjusted to bring the modeled CO_2 closer to the observed CO_2. The $CO2_{NEE}$ tracer is tracked by the model from the selected regions and the rest of the globe as shown in Figure 3 and can be expressed as

$$CO2_{NEE} = CO2_{NEE}^{M} + CO2_{NEE}^{S} + CO2_{NEE}^{T} + CO2_{NEE}^{global}, \tag{3}$$

with the right hand terms representing regional and the rest of the globe NEE CO_2 tracers. Only the regional tracers are adjusted in this study.

The optimization is performed at each of the three towers (M, S, and T) by solving for the minimum value of the cost function (Rodgers, 2000):

$$J(a) = \frac{1}{2}[(\hat{y} + \alpha CO2_{NEE}^{region}) - y]R^{-1}[(\hat{y} + \alpha CO2_{NEE}^{region}) - y]^{T} + \frac{1}{2}\alpha B^{-1}\alpha^{T}, \tag{4}$$

where α is a scaling factor by which NEE need to be changed, $\hat{y}$ is modeled 5-day running mean of daily afternoon (1500-1700 LST) averages of CO_2, y is observed 5-day running mean of daily afternoon (1500-1700 LST) averages of CO_2, B is the scaling factor error covariance term, and R is the observation-model error covariance matrix. B can be a matrix if more than one tracer is optimized, but in the current case of optimizing just one tracer, B becomes equivalent to $\sigma_{\alpha_p}^2 = 0.5$, which determines by how much the scaling factor α can be adjusted from the initial scaling factor $\alpha_p = 0$. R matrix represents combined observation-model error as well as the covariances among the days in each segment. The adjustment is performed on a total of 9 segments consisting of 15 daily y and $\hat{y}$ values to smooth out NEE daily variability over the time of about 2 weeks (Friend et al., 2007; Chevallier et al., 2012). Square matrix R is generated by first calculating observation-model daily error terms ε with the expression:

$$\varepsilon = y - \hat{y} - \overline{y - \hat{y}}. \tag{5}$$

Then ε terms are divided into 9 segments consisting of consecutive 15 daily values from the total of m daily values (in this case total is 135 days comprising the growing season of May-June-July-August-September or MJJAS). Variance is calculated for each segment as follows,

$$\sigma_i^2 = \frac{(\sum_{i=1}^{15} \varepsilon_i)^2}{15 - 1}. \tag{6}$$

This variance is unique to each segment and repeated for every day inside of an individual segment. Afterwards, the variance is converted to standard deviation σ (by taking a square root) and the initial version of R is

$$R = \begin{bmatrix} \sigma_1^2 & r_{12}\sigma_1\sigma_2 & \dots & r_{1m}\sigma_1\sigma_m \\ r_{21}\sigma_2\sigma_1 & \sigma_2^2 & \dots & r_{2m}\sigma_2\sigma_m \\ \vdots & \vdots & \ddots & \vdots \\ r_{m1}\sigma_m\sigma_1 & r_{m2}\sigma_m\sigma_2 & \dots & \sigma_m^2 \end{bmatrix}, \tag{7}$$

where the covariance terms representing propagation of error in time are modified by coefficient

$$r_{ij} = e^{-|i-j|/d}, \tag{8}$$

with d being a time scale. After the completion of the initial optimization, R is adjusted using reduced χ^2 statistic when initial term α becomes available for every segment with 9 being the total number of optimized segments,

$$\chi^2 = \frac{1}{9}[(\hat{y} + \alpha CO2_{NEE}^{region}) - y]R^{-1}[(\hat{y} + \alpha CO2_{NEE}^{region}) - y]^T. \tag{9}$$

For each segment, σ is modified until reduced χ^2 approximately approaches a value of 1 and final value of α is determined.

The cost function shown in equation 3 can be solved by the expression

$$\alpha = G(y - \hat{y}), \tag{10}$$

where G is the gain matrix defined as

$$G = B(CO2_{NEE}^{region})^T[CO2_{NEE}^{region}B(CO2_{NEE}^{region})^T + R]^{-1}. \tag{11}$$

Afterwards, the error covariance of α is estimated with

$$\hat{R} = [(CO2_{NEE}^{region})^T R^{-1} CO2_{NEE}^{region} + B^{-1}]^{-1}. \tag{12}$$

Once α is estimated, it is used to construct an optimized time series of CO_2 mole fractions along with its variation based on the estimated vector $\hat{R}$ (which provides 9 values of $\sigma_{optimized}$) by randomly drawing 1000 times from the normal distribution in the following fashion,

$$\alpha^* = \alpha + Normal(0, \sigma_{optimized}). \tag{13}$$

Then α and α^* are used to generate optimized CO_2 time series with the corresponding noise:

$$CO2_{optimized} = CO2_{model} + \alpha CO2_{NEE}^{region}, \tag{14}$$

$$CO2_{optimized}^* = CO2_{model} + \alpha^* CO2_{NEE}^{region}. \tag{15}$$

Afterwards, the adjusted NEE is estimated by summing the model NEE over all the pixels of each region (M, S, and T) and in 15-day increments and then using

$$NEE_{optimized}^{region} = NEE_{model}^{region} + \alpha NEE_{model}^{region}. \tag{16}$$

The total MJJAS NEE is found by adding all the 9 increments of each year. The uncertainties of 15-day segments are represented by the corresponding variance values from the $\hat{R}$ and uncertainties of the total MJJAS NEE are the sum of these variances.

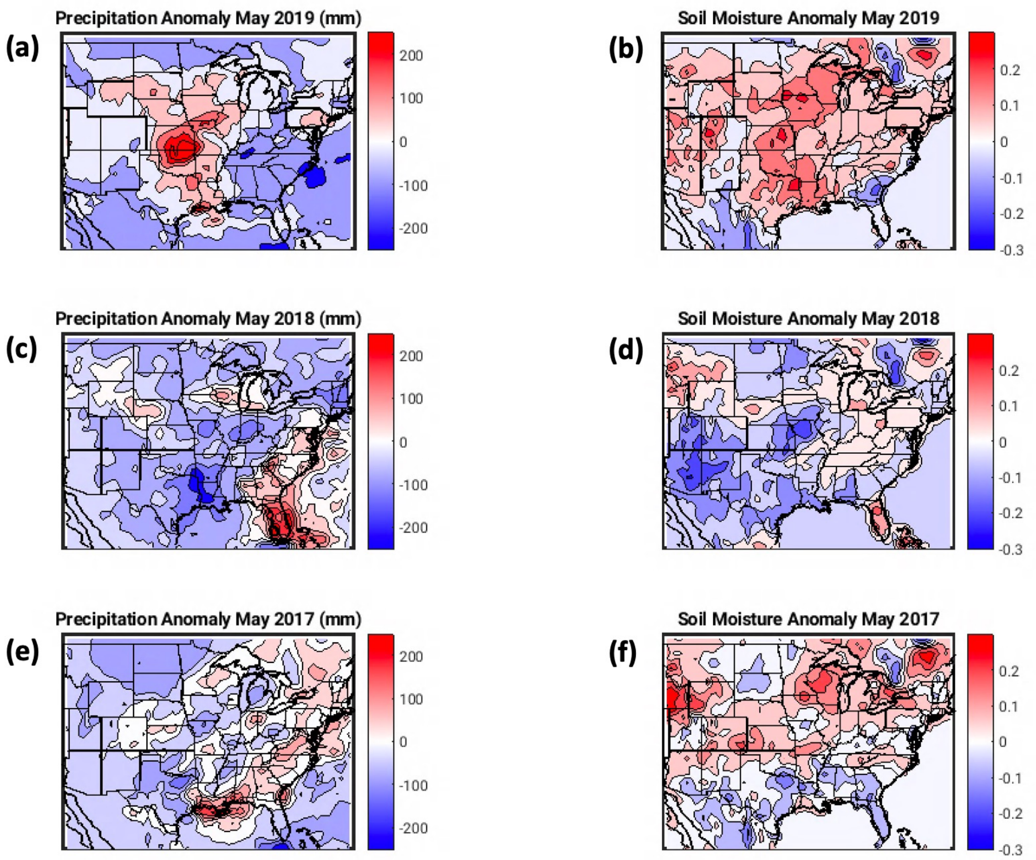

Figure 4. Precipitation and soil moisture May anomalies with respect to 1981-2010 climatology from MERRA-2 (Gelaro et al., 2017) in the eastern and central CONUS US for years 2017-2019, where panels (a), (c), and (e) correspond to precipitation anomalies over 2017-2019 and panels (b), (d), and (f) correspond to soil moisture anomalies over 2017-2019.

3 Results and Discussion

3.1 Precipitation, Soil Moisture Anomalies, and Effects on Crops

Figure 4 shows precipitation and soil moisture anomalies for the eastern and central CONUS over the years of 2017-2019 during the month of May when most of the flooding occurred. Comparing May precipitation totals over the years 2017-2019 indicates that 2019 (Figure 4a) saw significant positive anomalies in the central US including the Midwest and the South. The same regions in 2017 and 2018 (Figures 4e and 4c) generally saw negative anomalies except for southern Louisiana, Mississippi, and Alabama in 2017. Similarly, the soil moisture anomaly in May of 2019 (Figure 4b) is markedly positive in comparison to May of 2017 and 2018 (Figures 4f and 4d), although some positive anomalies can be seen in parts of the Midwest in 2017.

The immediate effects of 2019 flooding on the two major US crops is evident from Figure 5, where in Figures 5a and 5b planned planting of corn and soybeans was delayed by almost a month. The delay was likely caused by the severe waterlogging that occurred in early May not allowing farmers to proceed with the planned crop planting timetables. Figures 5c and 5d indicate that the total planted annual acres of corn and soy were about

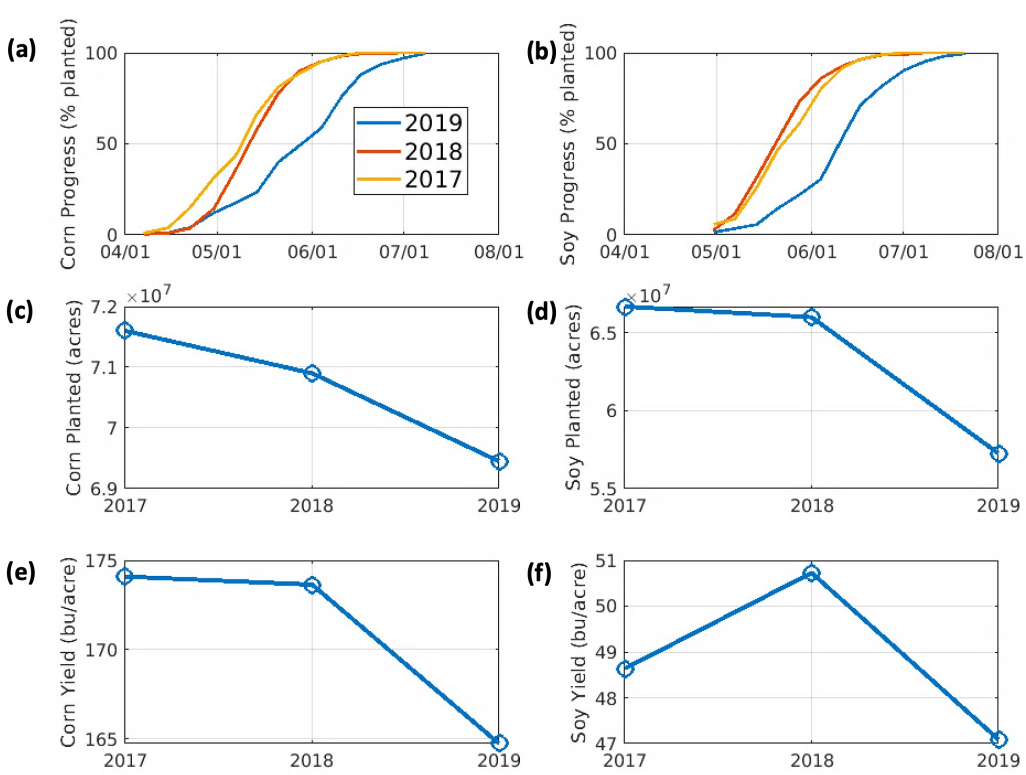

Figure 5. Corn and soybean statistics in the Midwestern states (listed in section 2.2) showing progress (percent planted), acres planted, and yield for the years 2017-2019, where (a), (c), and (e) indicate the mentioned statistics for corn and (b), (d), and (f) for soy (`https://quickstats.nass.usda.gov/`).

3-15% lower in 2019 than in years 2017 and 2018. Figures 5e and 5f show both corn and soy yields were lower in 2019 in comparison to 2017 and 2018.

The results described above suggest that the flooding event of 2019 was significant enough to cause noticeable reduction of crop yields in the Midwest compared to years 2017 and 2018, which may imply that the amount of carbon assimilated by the crops was also lower in 2019 than in the two prior years. This hypothesis will be addressed in the next section as well as the possible effects of the flooding on the non-crop vegetation.

3.2 NEE Optimization in the Midwest and the South

The optimization process explained in section 2.6 using WBI, MS (1 and 2), and WKT towers corresponding to regions M, S, and T produced 9 time series of the scaling factors for GEOS NEE CO_2 tracer mole fractions changing every 15 days over MJJAS time frame (total of 9 segments) for years 2017-2019 (Figure 6).

Region M scaling factors share some similar features over the 3 study years, albeit with somewhat different magnitudes. Figures 6a-c indicate that in the first 50-60 days LoFI net carbon uptake should be decreased and subsequently, net uptake should be increased except for 2018, where shortly after 100 days uptake should be slightly decreased again. These results suggest that for this geographic area there may be a mostly consistent model NEE bias.

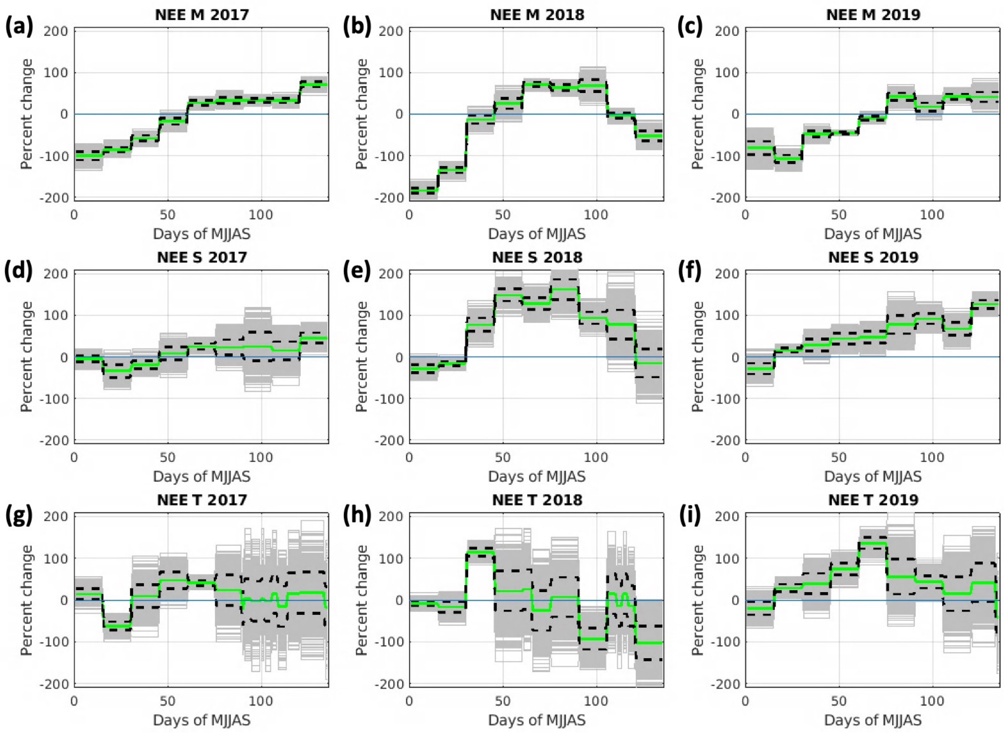

Figure 6. Scaling factors (shown in green) in percentages of GEOS NEE CO_2 tracer mole fractions as a function of 15-day period during MJJAS optimized using towers WBI, MS (1 and 2), and WKT located in M, S, and T regions, where (a) WBI in 2017, (b) WBI in 2018, (c) WBI in 2019, (d) MS-01 in 2017, (e) MS-02 in 2018, (d) MS-02 in 2019, (g) WKT in 2017, (h) WKT in 2018, (i) WKT in 2019. Black dashed lines indicate one sigma interval of an overall uncertainty (shown by the grey lines) of the estimated scaling factor. The scaling factors are plotted in such a way as to indicate a decrease in carbon uptake when the scaling factor is negative and to indicate an increase in carbon uptake when the scaling factor is positive.

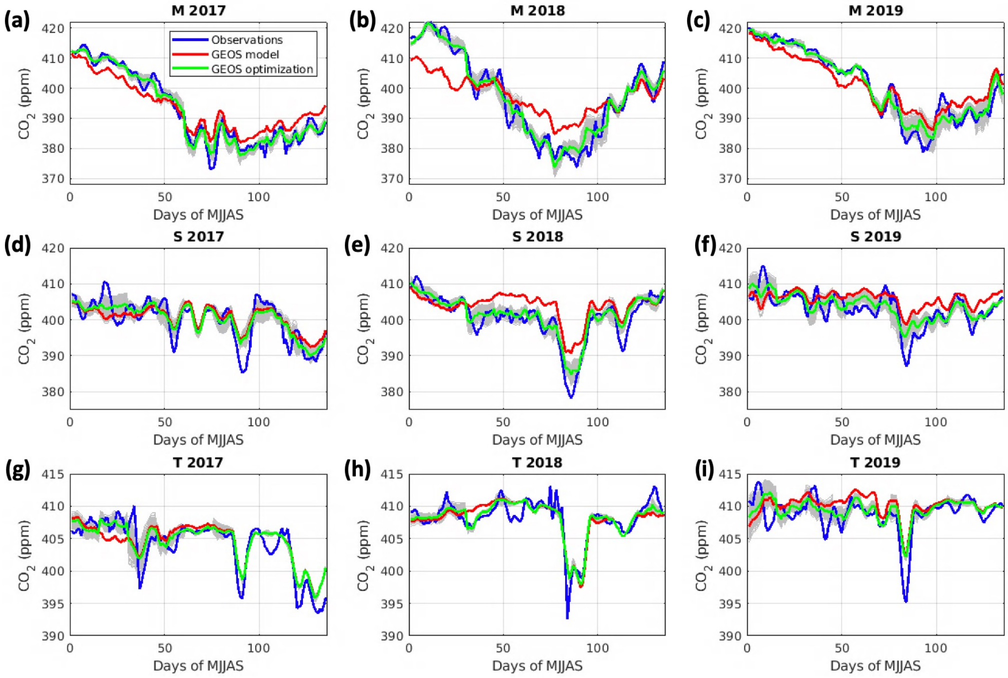

Figure 7. CO_2 in situ observations vs. GEOS model along with its optimization for towers WBI, MS (1 and 2), and WKT located in M, S, and T regions, where (a) WBI in 2017, (b) WBI in 2018, (c) WBI in 2019, (d) MS-01 in 2017, (e) MS-02 in 2018, (d) MS-02 in 2019, (g) WKT in 2017, (h) WKT in 2018, and (i) WKT in 2019. Grey lines indicate optimization uncertainty.

Moving on to the region S (Figures 6d-f), where the year 2017 is slightly different from the years 2018 and 2019, which can be explained by the fact that the 2017 optimization used a different MS tower. During 2017 the scaling factor is generally close to 0 and any adjustment seems to be characterized by high uncertainty. Interestingly, the year 2018 resembles the pattern seen in the Figure 6b although any decrease in the net carbon uptake is highly uncertain, whereas the increase in uptake is around 100-200% for the months of summer JJA. In 2019, there is a hint of the general increase in uptake throughout the whole MJJAS period, but with lesser magnitude than in 2018. Overall, it may be concluded that in the region S, the model tends to underestimate the land sink; however, the magnitude and time when this happens is somewhat less clear.

In the T region, the scaling factor tends to be noisy, varying up and down, except for June and July of 2019 where it is positive indicating the increase in net carbon uptake. The overall oscillatory nature of the scaling factor in the T region reflects the savannah/grasslands vegetation of the T region corresponding to the smaller values of NEE tracer that are hard to adjust effectively in comparison to the M and S regions.

The results of the optimization using the scaling factors shown in Figure 6 are demonstrated in the Figure 7, where the optimized GEOS CO_2 time series are compared to the original non-optimized GEOS CO_2 time series as well as to the tower observations. Like Figure 6, the time series are plotted over the days of MJJAS as 5-day running daily means for the regions M, S, and T and for the years 2017-2019.

With respect to the M region, the pattern of the scaling factors (shown in Figures 6a-c) applied to CO_2 time series in Figures 7a-c is evident as the model (red line) is too low in the first 50-60 days and afterwards it is generally too high. The model and the observations reveal a clear drawdown cycle of CO_2 in the middle of the summer attributable to the maturity of crops in that timeframe. The model tends to be too high (lacking carbon uptake) at those minima for all the examined years. An additional point of interest is the year 2018 with the model being 5-10 ppm low in the first 40 days - a significant discrepancy. It is possible that this can be explained by the negative soil moisture anomalies in May of 2018 in Iowa (Figure 4d), which may have had local effects on crops reducing uptake of carbon in comparison to 2017 or 2019 and were poorly identified by the model prior to optimization.

CO_2 time series (Figures 7d-f) in the S region show that the model tends to be too high in the years 2018 and 2019, whereas 2017 does not have this bias. This can be due to the fact that for 2017 optimization the MS-01 station was used, located in the southern part of Mississippi, while for 2018-2019 years MS-02 station was used, located in the northern part of Mississippi. One possible reason for differences between the stations is that MS-01 is closer to the Gulf Coast and therefore gets more of the tropical influence enhancing CO_2, while the MS-02 station is more influenced by the regional vegetation as there is more time for the tropical air to be depleted of CO_2 before reaching the tower. It is likely that the LoFI sink is not strong enough in the vicinity of MS-02.

Finally, the T region is characterized by generally flat CO_2 time series with occasional sudden dips (Figure 7g-i), which are also sometimes present in the S region. These dips are associated with the passage of cold fronts that can capture some of the Midwestern CO_2 depleted air during the summer and autumn months, but such fronts followed by the corresponding air mass do not occur often in the study period. As mentioned previously, the NEE tracer does not exhibit a clear cycle in the T region and therefore does not allow for much optimization. Part of 2019 may be an exception to that rule, as the model tends to be too high during the summer months and the optimization suggests that carbon uptake needs to be increased.

3.3 Optimization Validation

In this study, the validation is meant to gauge the tower representativeness of each respective region considered by evaluating determined adjustments of the GEOS simulation using independent-from-optimization observations. The optimization described in the previous section is validated with 3 towers INFLUX, LA-01, and AL-01, with data from the 2019 airborne ACT-America and 2019 shipboard SCOAPE campaigns. INFLUX tower results are demonstrated in the Figures 8a-c, where 5-day running daily averages of the observed, modeled, and model-adjusted CO_2 are plotted over the MJJAS period. Comparing Figures 7a-c and Figures 8a-c indicates that the GEOS model bias is generally similar for both WBI and INFLUX towers although with different magnitudes – too much uptake in the first 40 days of the growing season and too little uptake in the next 50-60 days. This result is reasonable as Indiana, like Iowa, is mainly an agriculture state (Figure 1). Therefore, the NEE optimization corrections (shown in green) adjust the model in the right direction. However, it is likely that the different vegetation in the proximity of INFLUX tower 1 (forests) and a somewhat different transport influence area affect the local CO_2 mole fractions.

Next, validation performed at LA-01 tower in years 2017 and 2018 is illustrated in Figures 8d and 8e. Validation at this tower serves to verify optimizations in both regions S and T. Unfortunately, a significant portion of the observed data is missing in 2017. It is possible to see that the correction of days 16-30 of MJJAS for 2017 (Figure 8d) resulting from the T region optimization (Figure 6g) is inconsistent with the Louisiana data. This discrepancy may imply that weekly CO_2 variability is not well captured by the optimization process and may vary considerably between S and T regions. In 2018, the corrections from the S and T regions optimizations (Figures 6e and 6h) are mostly consis-

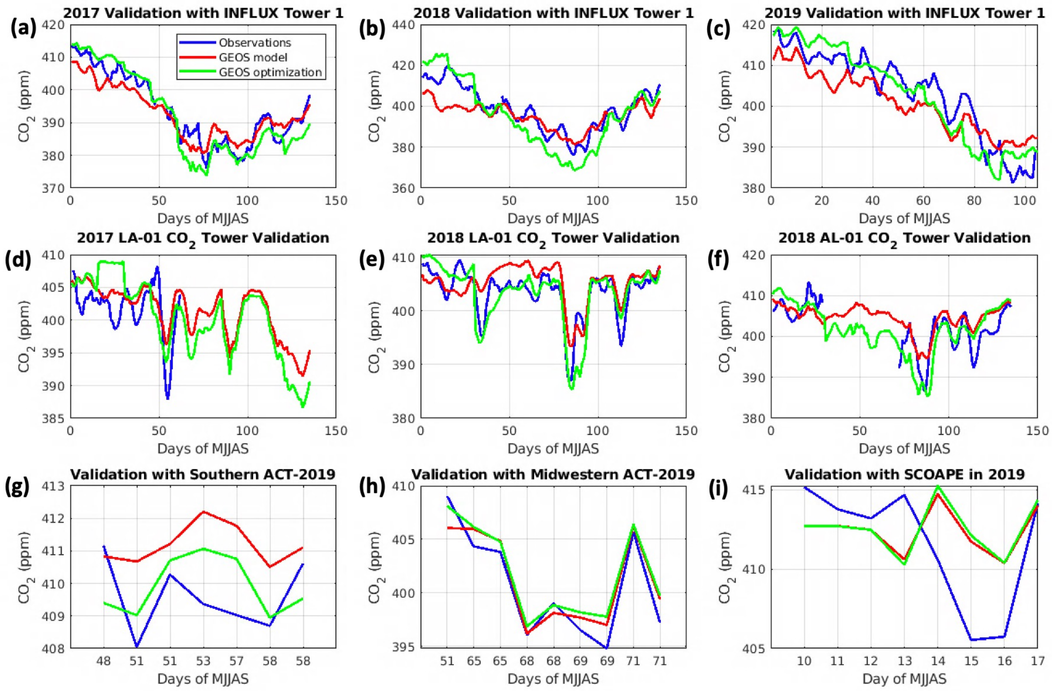

Figure 8. Validation of the optimization using various datasets throughout the years of interest, where the INFLUX tower 1 is shown in (a-c) for years 2017-2019, LA-01 tower is shown in (d-e) for years 2017-2018, AL-01 tower is shown in (f) for year 2018, southern ACT-2019 daily averaged flights are shown in (g), Midwestern ACT-2019 daily averaged flights are shown in (h), and shipboard campaign SCOAPE in 2019 is shown in (i).

tent with LA-01 (Figure 8e), suggesting that the original fluxes indeed generally underestimate regional carbon uptake in the given case.

The only data that is available from the AL-01 tower is for 2018 and at that it is incomplete. The AL-01 tower can partially validate the S region optimization. Figure 8f shows that in the first month the optimization is not helpful, but later in the period (starting at about day 90 of MJJAS) some improvement can be noted confirming higher carbon uptake. In this regard 2018 LA-01 and AL-01 towers are consistent and support the higher uptake values.

Finally, the two campaigns, airborne ACT-America 2019 and shipboard SCOAPE 2019, are used to validate the optimizations. ACT-America focused on all the regions of interest, first in the S and T regions during the second half of June and then in the M region during the first part of July. Figure 8g compares airborne CO_2 averages to corresponding original and adjusted model values. Noticeable improvement can be seen in the adjusted model, signaling that the S and T regions likely did experience higher carbon uptake than the original GEOS calculation showed. Regarding ACT-America flights in the M region denoted in Figure 8h, the original and adjusted models do not differ by much and generally closely resemble the airborne measurements. This is not surprising as Figure 6c suggests that in early July 2019 the model accurately estimated CO_2 mole fractions and did not require substantial adjustment. The SCOAPE 2019 shipboard measurements were of limited duration, taken in the middle of May 2019, and little could be learned from the comparisons as the optimization suggested only minor adjustment to the original fluxes used in this study. The SCOAPE observations suggest a massive carbon uptake during 14-17 days of MJJAS that did not extend to the location of the MS-02 tower in northern Mississippi. It is possible that some of the observed uptake was the result of the vegetation activity in parts of Florida, Georgia, Mississippi, and Alabama not well represented by the MS-02 tower. Additionally, this study did not consider any subtropical or tropical tracers, which may have played an important role in the CO_2 mole fractions observed by the ship.

Overall, the process of validating the optimizations showed that the derived scaling factors from the towers can be extended to the regions of interest albeit at times with a considerable error, which is difficult to quantify precisely. Established GEOS biases based on the WBI tower in the M region are partially observed at INFLUX tower 1. Regional ACT-America 2019 flights in the M region also indicate that the optimizations are reasonable. With regards to the S and T regions, towers LA-01 and AL-01 in 2018 and corresponding ACT-America 2019 flights show improved agreements with adjusted model fields. On the other hand, the LA-01 tower in 2017 and SCOAPE shipboard campaign in 2019 do not suggest any improvement; however, those are limited fragments of the overall validation dataset.

3.4 Growing Season NEE

Once the optimization and validation procedures are accomplished it is possible to adjust GEOS NEE and compare the net impact over the growing season. Figure 9 compares original GEOS and adjusted GEOS NEE for the M region over 15-day segments of MJJAS and whole MJJAS period during years 2017-2019. Examining the NEE totals over the growing season (Figure 9d) indicate that 2019 has the smallest NEE compared to 2017 and 2018 supporting the assertion that the 2019 flood did reduce overall crop carbon uptake in the M region. The result is captured by both the original GEOS and the optimized GEOS indicating that NEE component of the LoFI package is already somewhat sensitive to flooding, likely due to the use of MODIS remote sensing information. As noted previously, GEOS NEE exhibits consistent bias throughout the years 2017-2019, where the model uptakes too much carbon at the beginning of the growing season (May-June) and does not uptake enough later in the growing season specifically in

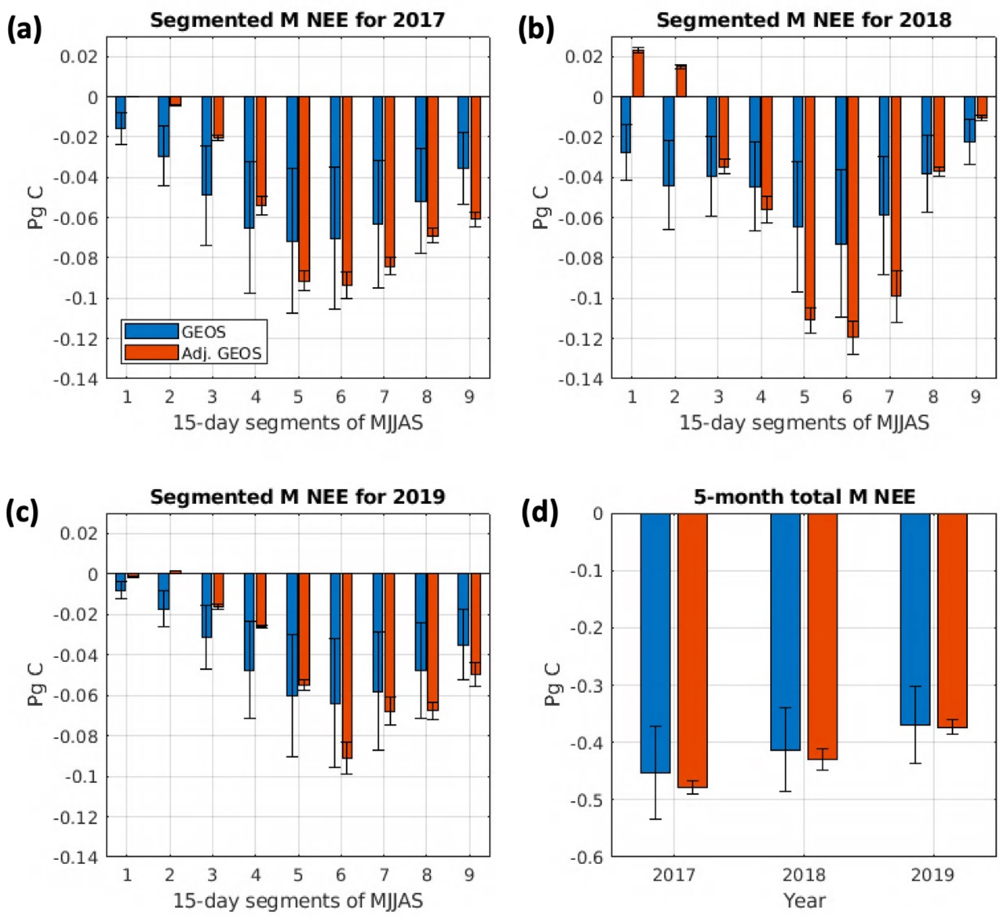

Figure 9. Original and adjusted GEOS NEE (in Pg of carbon) in the M region, where (a-c) panels show 15-day segments of the flux for years 2017-2019 and (d) summarizes MJJAS NEE flux for years 2017-2019. The uncertainty is one sigma.

July and August. This is specifically evident in Figure 9b where the optimization suggests a net carbon source in the first month of the growing season, which could be linked to the reduction in crop growth early in the growing season of 2018 due to a localized drought as evident from the Figures 5a and 4d (as was previously discussed in section 3.2).

The overall growing season magnitude of NEE in the S region (Figure 10) is approximately four times lower than that of the M region. It is hypothesized here that this difference between M and S regions be explained by the switch of vegetation from mostly crops to mixed forests and savannahs (Figure 1). In 2017 the optimization did not significantly alter GEOS model fluxes, while noticeable changes were observed in 2018 and 2019. It is important to note that the optimization for 2017 was carried out using tower MS-01 (southern Mississippi) and for years 2018 and 2019 tower MS-02 (northern Mississippi) was utilized. In years 2018 and 2019 the optimization implies that on average carbon uptake in the S region should be noticeably higher than what the original GEOS simulation indicates. That is especially true of 2018, where the total MJJAS uptake increased by about 30% after the adjustment. Out of all the examined years, 2019 reveals the highest growing season carbon uptake in the S region as evident from the Figure 10d.

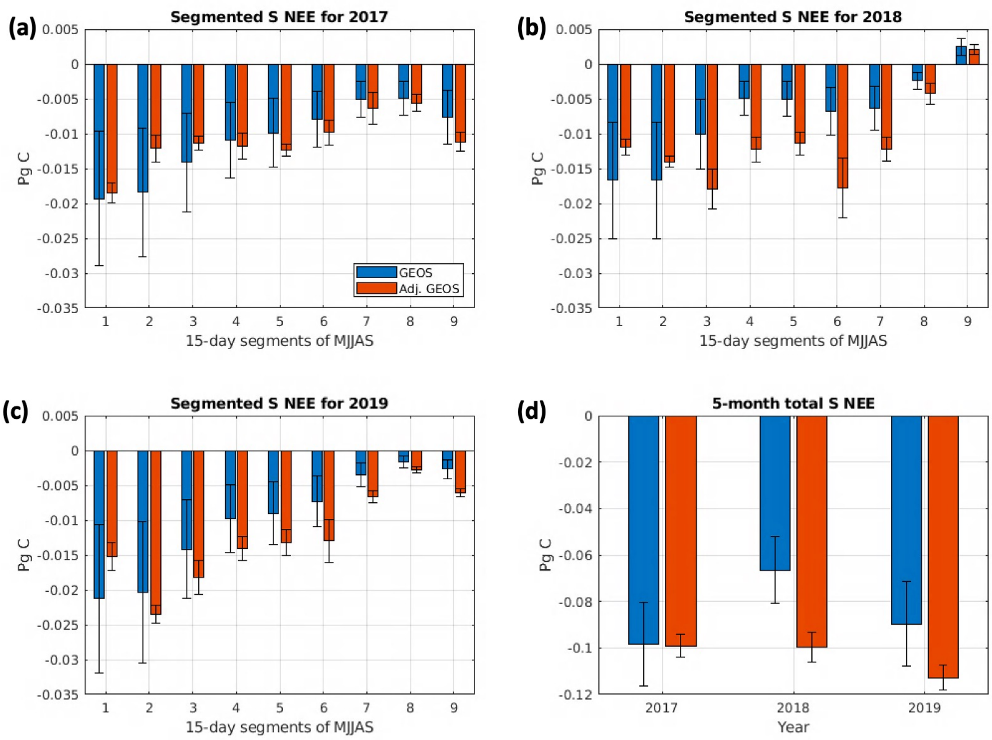

Figure 10. Original and adjusted GEOS NEE (in Pg of carbon) in the S region, where (a-c) panels show 15-day segments of the flux for years 2017-2019 and (d) summarizes MJJAS NEE flux for years 2017-2019. The uncertainty is one sigma.

This may indicate that the above-average rainfall of 2019 enhanced the regional plant growth, which is reflected by the higher than typical CO_2 drawdown.

The T region can be characterized by an even smaller NEE MJJAS variability in comparison to M and S regions reflecting the local vegetation consisting of grasslands and savannahs (Figure 1). Figure 11 shows generally little adjustments especially in years 2017 and 2018. In 2018, optimization suggests a slight decrease in uptake, but it is marred by a noticeable uncertainty. The most interesting results come from the 2019 optimization, apparent in Figures 11c and 11e, where there is a clear signal in the increased uptake. This is consistent with the signal determined in the S region for 2019 (Figure 10d). Both outcomes support the possibility that in this case the anomalous precipitation event in the late spring/early summer of 2019 contributed to higher carbon uptake in comparison to years 2017 and 2018.

4 Conclusions

Generally prolonged excessive water conditions will negatively influence a plant system causing anoxia (Zhou et al., 2020); however, the effects of flooding on an ecosystem are not straightforward and largely depend on a particular vegetation type and degree of waterlogging (Detmers et al., 2015; Sun et al., 2022). Wet conditions can result in an increase of carbon net uptake, but too much wetness may lead to a net carbon release because in these conditions both productivity and respiration tend to decrease, and the overall NEE balance will be contingent on specific environmental conditions (Ahlström et al., 2015; Bloch & Bhattacharjee, 2020). The current study affirms the mentioned as-

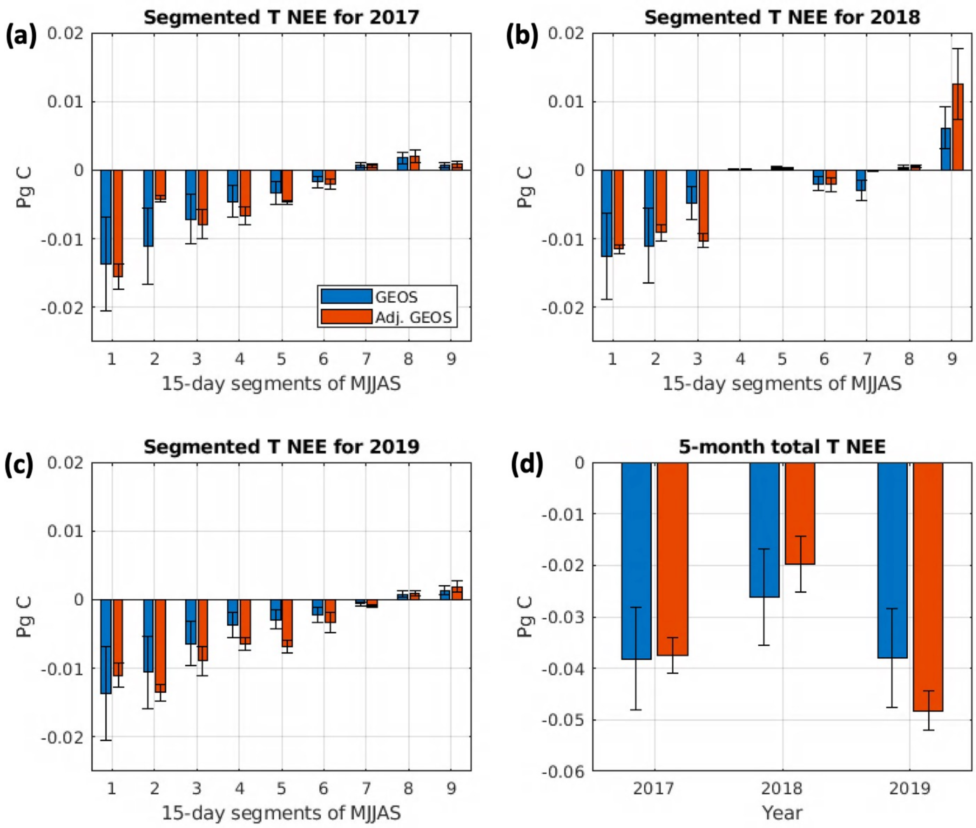

Figure 11. Original and adjusted GEOS NEE (in Pg of carbon) in the T region, where (a-c) panels show 15-day segments of the flux for years 2017-2019 and (d) summarizes MJJAS NEE flux for years 2017-2019. The uncertainty is one sigma.

sertions and implies that crops such as corn and soybeans seem to be more susceptible to waterlogging than non-crop vegetation such as savannahs, forests, and grasslands. This is expressed in the reduced carbon uptake in the first part of the growing season over the Midwestern region of the US (mainly crops) and overall increased carbon uptake in the Southern region of the US (mainly non-crop) during the flood of 2019 when compared to 2017 and 2018. The change in 2019 growing season NEE in the Midwest with respect to 2017 and 2018 of about 0.1 Pg C exceeded the total magnitude of NEE in region T (-0.05 Pg C) and equaled to the total magnitude of NEE in region S (-0.1 Pg C). For the perspective, an annual average NEE over the years 2010-2019 in North America is about -0.5 Pg C (Jiang et al., 2022). In addition, significant slowdown of the crop planting progress occurred in the early growing season of 2019 as most of the corn and soybeans in the US are in the Midwest. Flooding impacts in managed ecosystems dominated the net effect for the 2019 event. As humans are considering a variety of strategies to tackle climate change, sustainable crop management practice can accelerate carbon input into the soil (Meena et al., 2020). The exact effect of flooding on such practices is unclear but the delay in planting of crops explored in the current work raises questions that could influence future carbon balance and should be considered in strategies to reduce net emissions.

The impact of flooding on NEE and atmospheric CO_2 is readily observed by satellites (Yin et al., 2020) and a variety of in situ observational approaches (this study). Like Yin et al., (2020), for the Midwestern region this study finds a decrease in net carbon uptake over June and July of 2019 of about 0.07-1.3 PgC [roughly 14-26% of an average annual carbon net uptake in North America (Jiang et al., 2022)] when compared to both 2017 and 2018 and an increase in net carbon uptake in August and September of near 0.04 PgC (roughly 8% of an average annual carbon net uptake in North America) when compared to 2018 [Note that Yin et al. (2020) estimated Gross Primary Production (GPP), which does not account for RE, while this study estimated NEE]. However, the results from the current study suggest that comparing 2019 to 2018 may not be optimal as 2018 may not be representative of an average growing season carbon activity (Jiang et al., 2022). For instance, assessment of 2019 NEE values with 2017 NEE values does not seem to show a "recovery" in August-September time frame as stated in Yin et al. (2020) suggesting that additional inquiries are required into the detailed effects of flooding on the carbon uptake. Atmospheric CO_2 observations can play an important role in helping to monitor the impact of agricultural systems but require sustained planning and coordination (e.g., the discontinuity in towers made this study more difficult).

Overall, the low latency flux estimation approach from LoFI is credible in discerning flooding and non-flooding events, which demonstrates the maturity of modeling tools that can be applied to carbon monitoring at the current stage. Further investigations in this direction are imperative as only a sparse amount of literature is available regarding carbon exchange between an ecosystem and the atmosphere in a variety of water-excess conditions.

5 Acknowledgements

This work is supported by NASA's Carbon Monitoring System (NNH16DA001N-CMS 16-CMS16-0054, NNH20DA001N-CMS 20-CMS20-0011), NASA Postdoctoral Program (NPP), and a contract appointment with Earth System Science Interdisciplinary Center (ESSIC) at University of Maryland (UMD). We thank NASA Goddard Space Flight Center (GSFC) facility for providing us with the tools needed to perform the simulations used in this work. Also, we wish to thank ACT-America and SCOAPE teams for helping us with specific questions pertinent to the data used in the current study.

6 Open Research

Data Availability Statement

CO_2 data from MS-01, MS-02, AL-01, and LA-01 towers are available at `https://sites.psu.edu/gulfcoast/data/`; also see Miles et al. (2018). WBI and WKT tower data are available here: `https://gml.noaa.gov/ccgg/obspack/index.html`. All of the crop data used in this article can be found at `https://quickstats.nass.usda.gov/`. ACT airborne data are located at `https://actamerica.ornl.gov/airborne_data.shtml`. SCOAPE data are stored at `https://www-air.larc.nasa.gov/missions/scoape/index.html`. MERRA-2 data used for GEOS forcing, precipitation and soil moisture analyzes are available at `https://gmao.gsfc.nasa.gov/reanalysis/MERRA-2/`. Source code for the NASA GEOS model is available under the NASA Open-Source Agreement at `http://opensource.gsfc.nasa.gov/projects/GEOS-5`. The NEE fluxes used in GEOS are based on the CASA-GFED dataset provided at GES DISC (`https://disc.gsfc.nasa.gov/datasets/GEOS_CASAGFED_3H_NEE_3/summary`).

More extensive descriptions of tower and airborne data can be found in Wei et al. (2021) and Masarie et al. (2014).

References

Ahlström, A., Raupach, M. R., Schurgers, G., Smith, B., Arneth, A., Jung, M., ... Zeng, N. (2015). The dominant role of semi-arid ecosystems in the trend and variability of the land CO_2 sink. *Science*, *348*(6237), 895-899. Retrieved from `https://www.science.org/doi/abs/10.1126/science.aaa1668` doi: 10.1126/science.aaa1668

Ahmed, F., Rafii, M., Ismail, M. R., Juraimi, A. S., Rahim, H., Asfaliza, R., & Latif, M. A. (2013). Waterlogging tolerance of crops: breeding, mechanism of tolerance, molecular approaches, and future prospects. *BioMed research international*, *2013*.

Andrews, A. E., Kofler, J. D., Trudeau, M. E., Williams, J. C., Neff, D. H., Masarie, K. A., ... Tans, P. P. (2014). CO_2, CO, and CH_4 measurements from tall towers in the noaa earth system research laboratory's global greenhouse gas reference network: instrumentation, uncertainty analysis, and recommendations for future high-accuracy greenhouse gas monitoring efforts. *Atmospheric Measurement Techniques*, *7*(2), 647–687. Retrieved from `https://amt.copernicus.org/articles/7/647/2014/` doi: 10.5194/amt-7-647-2014

Bloch, M., & Bhattacharjee, J. (2020). Characterizing the carbon fluxes of a bottomland hardwood forest. In *Agu fall meeting abstracts* (Vol. 2020, pp. B065–0004).

Bourtsoukidis, E., Kawaletz, H., Radacki, D., Schütz, S., Hakola, H., Hellén, H., ... Bonn, B. (2014). Impact of flooding and drought conditions on the emission of volatile organic compounds of quercus robur and prunus serotina. *Trees*, *28*(1), 193–204.

Chevallier, F., Wang, T., Ciais, P., Maignan, F., Bocquet, M., Altaf Arain, M., ... Moors, E. J. (2012). What eddy-covariance measurements tell us about prior land flux errors in CO_2-flux inversion schemes. *Global Biogeochemical Cycles*, *26*(1). Retrieved from `https://agupubs.onlinelibrary.wiley.com/doi/abs/10.1029/2010GB003974` doi: https://doi.org/10.1029/2010GB003974

Dalmagro, H. J., Zanella de Arruda, P. H., Vourlitis, G. L., Lathuillière, M. J., de S. Nogueira, J., Couto, E. G., & Johnson, M. S. (2019). Radiative forcing of methane fluxes offsets net carbon dioxide uptake for a tropical flooded forest. *Global Change Biology*, *25*(6), 1967-1981. Retrieved from `https://onlinelibrary.wiley.com/doi/abs/10.1111/gcb.14615` doi:

https://doi.org/10.1111/gcb.14615

Davis, K. J., Browell, E. V., Feng, S., Lauvaux, T., Obland, M. D., Pal, S., ... Williams, C. A. (2021). The atmospheric carbon and transport (ACT)-america mission. *Bulletin of the American Meteorological Society*, *102*(9), E1714 - E1734. Retrieved from https://journals.ametsoc.org/view/journals/bams/102/9/BAMS-D-20-0300.1.xml doi: 10.1175/BAMS-D-20-0300.1

Davis, K. J., Deng, A., Lauvaux, T., Miles, N. L., Richardson, S. J., Sarmiento, D. P., ... Karion, A. (2017, 05). The Indianapolis Flux Experiment (INFLUX): A test-bed for developing urban greenhouse gas emission measurements. *Elementa: Science of the Anthropocene*, *5*. Retrieved from https://doi.org/10.1525/elementa.188 (21) doi: 10.1525/elementa.188

Detmers, R. G., Hasekamp, O., Aben, I., Houweling, S., van Leeuwen, T. T., Butz, A., ... Poulter, B. (2015). Anomalous carbon uptake in australia as seen by GOSAT. *Geophysical Research Letters*, *42*(19), 8177-8184. Retrieved from https://agupubs.onlinelibrary.wiley.com/doi/abs/10.1002/2015GL065161 doi: https://doi.org/10.1002/2015GL065161

Dinsmore, K. J., Billett, M. F., & Dyson, K. E. (2013). Temperature and precipitation drive temporal variability in aquatic carbon and ghg concentrations and fluxes in a peatland catchment. *Global Change Biology*, *19*(7), 2133-2148. Retrieved from https://onlinelibrary.wiley.com/doi/abs/10.1111/gcb.12209 doi: https://doi.org/10.1111/gcb.12209

Dlugokencky, E., & Tans, P. (2016). *The marine boundary layer reference (downloaded early 2016).*

Dušek, J., Čížková, H., Czerný, R., Taufarová, K., Šmídová, M., & Janouš, D. (2009). Influence of summer flood on the net ecosystem exchange of CO_2 in a temperate sedge-grass marsh. *Agricultural and Forest Meteorology*, *149*(9), 1524-1530. Retrieved from https://www.sciencedirect.com/science/article/pii/S0168192309000951 doi: https://doi.org/10.1016/j.agrformet.2009.04.007

Follett, R. (2001). Soil management concepts and carbon sequestration in cropland soils. *Soil and Tillage Research*, *61*(1), 77-92. Retrieved from https://www.sciencedirect.com/science/article/pii/S0167198701001805 (XVth ISTRO Conference on Tillage at the Threshold of the 21st Century: Looking Ahead) doi: https://doi.org/10.1016/S0167-1987(01)00180-5

Frank, D., Reichstein, M., Bahn, M., Thonicke, K., Frank, D., Mahecha, M. D., ... Zscheischler, J. (2015). Effects of climate extremes on the terrestrial carbon cycle: concepts, processes and potential future impacts. *Global Change Biology*, *21*(8), 2861-2880. Retrieved from https://onlinelibrary.wiley.com/doi/abs/10.1111/gcb.12916 doi: https://doi.org/10.1111/gcb.12916

Friend, A. D., ARNETH, A., KIANG, N. Y., LOMAS, M., OGÉE, J., RÖDENBECK, C., ... ZAEHLE, S. (2007). Fluxnet and modelling the global carbon cycle. *Global Change Biology*, *13*(3), 610-633. Retrieved from https://onlinelibrary.wiley.com/doi/abs/10.1111/j.1365-2486.2006.01223.x doi: https://doi.org/10.1111/j.1365-2486.2006.01223.x

Gelaro, R., McCarty, W., Suárez, M. J., Todling, R., Molod, A., Takacs, L., ... Zhao, B. (2017). The modern-era retrospective analysis for research and applications, version 2 (MERRA-2). *Journal of Climate*, *30*(14), 5419 - 5454. Retrieved from https://journals.ametsoc.org/view/journals/clim/30/14/jcli-d-16-0758.1.xml doi: 10.1175/JCLI-D-16-0758.1

Han, G., Chu, X., Xing, Q., Li, D., Yu, J., Luo, Y., ... Rafique, R. (2015). Effects of episodic flooding on the net ecosystem CO_2 exchange of a supratidal wetland in the yellow river delta. *Journal of Geophysical Research: Biogeosciences*, *120*(8), 1506-1520. Retrieved from https://agupubs.onlinelibrary.wiley.com/doi/abs/10.1002/2015JG002923 doi: https://doi.org/10.1002/2015JG002923

Hilton, R. G., Galy, A., Hovius, N., Chen, M.-C., Horng, M.-J., & Chen, H. (2008). Tropical-cyclone-driven erosion of the terrestrial biosphere from mountains. *nature Geoscience*, *1*(11), 759–762.

Jiang, F., Ju, W., He, W., Wu, M., Wang, H., Wang, J., ... Chen, J. M. (2022). A 10-year global monthly averaged terrestrial net ecosystem exchange dataset inferred from the ACOS GOSAT v9 XCO_2 retrievals (GCAS2021). *Earth System Science Data*, *14*(7), 3013–3037. Retrieved from `https://essd.copernicus.org/articles/14/3013/2022/` doi: 10.5194/essd-14-3013-2022

Knapp, A. K., Beier, C., Briske, D. D., Classen, A. T., Luo, Y., Reichstein, M., ... Weng, E. (2008, 10). Consequences of More Extreme Precipitation Regimes for Terrestrial Ecosystems. *BioScience*, *58*(9), 811-821. Retrieved from `https://doi.org/10.1641/B580908` doi: 10.1641/B580908

Koster, R. D., Darmenov, A. S., & da Silva, A. M. (2015). *The quick fire emissions dataset (QFED): Documentation of versions 2.1, 2.2 and 2.4* (Tech. Rep.).

Kramer, K., Vreugdenhil, S. J., & van der Werf, D. (2008). Effects of flooding on the recruitment, damage and mortality of riparian tree species: A field and simulation study on the rhine floodplain. *Forest Ecology and Management*, *255*(11), 3893-3903. Retrieved from `https://www.sciencedirect.com/science/article/pii/S0378112708002922` doi: https://doi.org/10.1016/j.foreco.2008.03.044

Lal, R. (2019). Accelerated soil erosion as a source of atmospheric CO_2. *Soil and Tillage Research*, *188*, 35-40. Retrieved from `https://www.sciencedirect.com/science/article/pii/S0167198718300345` (Soil Carbon and Climate Change: the 4 per Mille Initiative) doi: https://doi.org/10.1016/j.still.2018.02.001

Masarie, K. A., Peters, W., Jacobson, A. R., & Tans, P. P. (2014). Obspack: a framework for the preparation, delivery, and attribution of atmospheric greenhouse gas measurements. *Earth System Science Data*, *6*(2), 375–384. Retrieved from `https://essd.copernicus.org/articles/6/375/2014/` doi: 10.5194/essd-6-375-2014

Masarie, K. A., & Tans, P. P. (1995). Extension and integration of atmospheric carbon dioxide data into a globally consistent measurement record. *Journal of Geophysical Research: Atmospheres*, *100*(D6), 11593-11610. Retrieved from `https://agupubs.onlinelibrary.wiley.com/doi/abs/10.1029/95JD00859` doi: https://doi.org/10.1029/95JD00859

Meena, R. S., Kumar, S., & Yadav, G. S. (2020). Soil carbon sequestration in crop production. In R. S. Meena (Ed.), *Nutrient dynamics for sustainable crop production* (pp. 1–39). Singapore: Springer Singapore. Retrieved from `https://doi.org/10.1007/978-981-13-8660-2_1` doi: 10.1007/978-981-13-8660-2_1

Miles, N., Richardson, S., Martins, D., Davis, K., Lauvaux, T., Haupt, B., & Miller, S. (2018). *Act-america: L2 in situ CO_2, CO, and CH_4 concentrations from towers, eastern USA. ornl daac, oak ridge, tennessee, usa.*

Miyata, A., Leuning, R., Denmead, O. T., Kim, J., & Harazono, Y. (2000). Carbon dioxide and methane fluxes from an intermittently flooded paddy field. *Agricultural and Forest Meteorology*, *102*(4), 287-303. Retrieved from `https://www.sciencedirect.com/science/article/pii/S0168192300000927` doi: https://doi.org/10.1016/S0168-1923(00)00092-7

Molod, A., Takacs, L., Suarez, M., & Bacmeister, J. (2015). Development of the GEOS-5 atmospheric general circulation model: evolution from MERRA to MERRA2. *Geoscientific Model Development*, *8*(5), 1339–1356. Retrieved from `https://gmd.copernicus.org/articles/8/1339/2015/` doi: 10.5194/gmd-8-1339-2015

Neri, A., Villarini, G., & Napolitano, F. (2020). Intraseasonal predictability of the duration of flooding above national weather service flood warning levels across the U.S. midwest. *Hydrological Processes*, *34*(23), 4505-4511. Retrieved from https://onlinelibrary.wiley.com/doi/abs/10.1002/hyp.13902 doi: https://doi.org/10.1002/hyp.13902

Oda, T., & Maksyutov, S. (2015). ODIAC fossil fuel CO_2 emissions dataset (version name: ODIAC2016). *Center for Global Environmental Research, National Institute for Environmental Studies, https://doi. org/10.17595/20170411.001*.

Oda, T., Maksyutov, S., & Andres, R. J. (2018). The open-source data inventory for anthropogenic co_2, version 2016 (odiac2016): a global monthly fossil fuel co_2 gridded emissions data product for tracer transport simulations and surface flux inversions. *Earth System Science Data*, *10*(1), 87–107. Retrieved from https://essd.copernicus.org/articles/10/87/2018/ doi: 10.5194/essd-10-87-2018

Ott, L. E., Pawson, S., Collatz, G. J., Gregg, W. W., Menemenlis, D., Brix, H., ... Kawa, S. R. (2015). Assessing the magnitude of CO_2 flux uncertainty in atmospheric CO_2 records using products from nasa's carbon monitoring flux pilot project. *Journal of Geophysical Research: Atmospheres*, *120*(2), 734-765. Retrieved from https://agupubs.onlinelibrary.wiley.com/doi/abs/10.1002/2014JD022411 doi: https://doi.org/10.1002/2014JD022411

Paustian, K., Six, J., Elliott, E., & Hunt, H. (2000). Management options for reducing CO_2 emissions from agricultural soils. *Biogeochemistry*, *48*(1), 147–163.

Price, J. J., & Berkowitz, J. F. (2020). Wetland functional responses to prolonged inundation in the active mississippi river floodplain. *Wetlands*, *40*(6), 1949–1956.

Randerson, J. T., Thompson, M. V., Malmstrom, C. M., Field, C. B., & Fung, I. Y. (1996). Substrate limitations for heterotrophs: Implications for models that estimate the seasonal cycle of atmospheric CO_2. *Global Biogeochemical Cycles*, *10*(4), 585-602. Retrieved from https://agupubs.onlinelibrary.wiley.com/doi/abs/10.1029/96GB01981 doi: https://doi.org/10.1029/96GB01981

Reed, T., Mason, L. R., & Ekenga, C. C. (2020). Adapting to climate change in the upper mississippi river basin: Exploring stakeholder perspectives on river system management and flood risk reduction. *Environmental Health Insights*, *14*, 1178630220984153. Retrieved from https://doi.org/10.1177/1178630220984153 (PMID: 33447043) doi: 10.1177/1178630220984153

Reichle, R. H., Draper, C. S., Liu, Q., Girotto, M., Mahanama, S. P., Koster, R. D., & De Lannoy, G. J. (2017). Assessment of MERRA-2 land surface hydrology estimates. *Journal of Climate*, *30*(8), 2937–2960.

Reichle, R. H., Liu, Q., Koster, R. D., Draper, C. S., Mahanama, S. P., & Partyka, G. S. (2017). Land surface precipitation in MERRA-2. *Journal of Climate*, *30*(5), 1643–1664.

Reichstein, M., Bahn, M., Ciais, P., Frank, D., Mahecha, M. D., Seneviratne, S. I., ... others (2013). Climate extremes and the carbon cycle. *Nature*, *500*(7462), 287–295.

Rodgers, C. D. (2000). *Inverse methods for atmospheric sounding: theory and practice* (Vol. 2). World scientific.

Rosenzweig, C., Tubiello, F. N., Goldberg, R., Mills, E., & Bloomfield, J. (2002). Increased crop damage in the us from excess precipitation under climate change. *Global Environmental Change*, *12*(3), 197-202. Retrieved from https://www.sciencedirect.com/science/article/pii/S0959378002000080 doi: https://doi.org/10.1016/S0959-3780(02)00008-0

Schuldt, K. N., Mund, M., Luijkx, I. T., Aalto, T., Abshire, J. B., Aikin, K., ... others (2021). Multi-laboratory compilation of atmospheric carbon dioxide data for the period 1957–2019, obspack_co2_1_GLOBALVIEWplus_v6.1_2021-03-01, NOAA earth system research laboratory, global monitoring laboratory [data set]. *NOAA Earth System Research Laboratory, Global Monitoring Laboratory [data set]*, *10*, 20210801.

Schwalm, C. R., Williams, C. A., Schaefer, K., Baldocchi, D., Black, T. A., Goldstein, A. H., … Scott, R. L. (2012). Reduction in carbon uptake during turn of the century drought in western north america. *Nature Geoscience*, *5*(8), 551–556.

Stein, A. F., Draxler, R. R., Rolph, G. D., Stunder, B. J. B., Cohen, M. D., & Ngan, F. (2015). NOAA's HYSPLIT atmospheric transport and dispersion modeling system. *Bulletin of the American Meteorological Society*, *96*(12), 2059 - 2077. Retrieved from https://journals.ametsoc.org/view/journals/bams/96/12/bams-d-14-00110.1.xml doi: 10.1175/BAMS-D-14-00110.1

Sulla-Menashe, D., & Friedl, M. A. (2018). User guide to collection 6 MODIS land cover (MCD12q1 and MCD12C1) product. *USGS: Reston, VA, USA*, *1*, 18.

Sun, B., Jiang, M., Han, G., Zhang, L., Zhou, J., Bian, C., … Xia, J. (2022). Experimental warming reduces ecosystem resistance and resilience to severe flooding in a wetland. *Science Advances*, *8*(4), eabl9526. Retrieved from https://www.science.org/doi/abs/10.1126/sciadv.abl9526 doi: 10.1126/sciadv.abl9526

Thompson, A. M. (2020). *Evaluation of NASA's remote-sensing capabilities in coastal environments* (Tech. Rep.). Dept of Interior-Bureau of Ocean Energy Management (BOEM).

van der Molen, M., Dolman, A., Ciais, P., Eglin, T., Gobron, N., Law, B., … Wang, G. (2011). Drought and ecosystem carbon cycling. *Agricultural and Forest Meteorology*, *151*(7), 765-773. Retrieved from https://www.sciencedirect.com/science/article/pii/S0168192311000517 doi: https://doi.org/10.1016/j.agrformet.2011.01.018

van der Werf, G. R., Randerson, J. T., Giglio, L., Collatz, G. J., Mu, M., Kasibhatla, P. S., … van Leeuwen, T. T. (2010). Global fire emissions and the contribution of deforestation, savanna, forest, agricultural, and peat fires (1997–2009). *Atmospheric Chemistry and Physics*, *10*(23), 11707–11735. Retrieved from https://acp.copernicus.org/articles/10/11707/2010/ doi: 10.5194/acp-10-11707-2010

Wei, Y., Shrestha, R., Pal, S., Gerken, T., Feng, S., McNelis, J., … Davis, K. J. (2021). Atmospheric carbon and transport – america (ACT-america) data sets: Description, management, and delivery. *Earth and Space Science*, *8*(7), e2020EA001634. Retrieved from https://agupubs.onlinelibrary.wiley.com/doi/abs/10.1029/2020EA001634 (e2020EA001634 2020EA001634) doi: https://doi.org/10.1029/2020EA001634

Weir, B., Ott, L. E., Collatz, G. J., Kawa, S. R., Poulter, B., Chatterjee, A., … Pawson, S. (2021). Bias-correcting carbon fluxes derived from land-surface satellite data for retrospective and near-real-time assimilation systems. *Atmospheric Chemistry and Physics*, *21*(12), 9609–9628. Retrieved from https://acp.copernicus.org/articles/21/9609/2021/ doi: 10.5194/acp-21-9609-2021

Yildirim, E., & Demir, I. (2022). Agricultural flood vulnerability assessment and risk quantification in iowa. *Science of The Total Environment*, *826*, 154165. Retrieved from https://www.sciencedirect.com/science/article/pii/S0048969722012578 doi: https://doi.org/10.1016/j.scitotenv.2022.154165

Yin, Y., Byrne, B., Liu, J., Wennberg, P. O., Davis, K. J., Magney, T., … Frankenberg, C. (2020). Cropland carbon uptake delayed and reduced by 2019 midwest floods. *AGU Advances*, *1*(1), e2019AV000140. Retrieved from https://agupubs.onlinelibrary.wiley.com/doi/abs/10.1029/2019AV000140 (e2019AV000140 2019AV000140) doi: https://doi.org/10.1029/2019AV000140

Zaerr, J. B. (1983, 03). Short-Term Flooding and Net Photosynthesis in Seedlings of Three Conifers. *Forest Science*, *29*(1), 71-78. Retrieved from https://doi.org/10.1093/forestscience/29.1.71 doi: 10.1093/forestscience/29.1.71

Zhang, W., & Villarini, G. (2021). Greenhouse gases drove the increasing trends in spring precipitation across the central USA. *Philosophical Transactions of the Royal Society A: Mathematical, Physical and Engineering Sciences*, *379*(2195), 20190553. Retrieved from https://royalsocietypublishing.org/doi/abs/10.1098/rsta.2019.0553 doi: 10.1098/rsta.2019.0553

Zhou, W., Chen, F., Meng, Y., Chandrasekaran, U., Luo, X., Yang, W., & Shu, K. (2020). Plant waterlogging/flooding stress responses: From seed germination to maturation. *Plant Physiology and Biochemistry*, *148*, 228-236. Retrieved from https://www.sciencedirect.com/science/article/pii/S0981942820300206 doi: https://doi.org/10.1016/j.plaphy.2020.01.020

Zomer, R. J., Bossio, D. A., Sommer, R., & Verchot, L. V. (2017). Global sequestration potential of increased organic carbon in cropland soils. *Scientific Reports*, *7*(1), 1–8.

Zona, D., Lipson, D. A., Paw U, K. T., Oberbauer, S. F., Olivas, P., Gioli, B., & Oechel, W. C. (2012). Increased CO_2 loss from vegetated drained lake tundra ecosystems due to flooding. *Global Biogeochemical Cycles*, *26*(2). Retrieved from https://agupubs.onlinelibrary.wiley.com/doi/abs/10.1029/2011GB004037 doi: https://doi.org/10.1029/2011GB004037